Prepared for submission to JHEP
UTTG-11-18

Rotating traversable wormholes in AdS

Elena Caceres,[a] **Anderson Seigo Misobuchi,**[a] **Ming-Lei Xiao**[b]

[a] *Theory Group, Department of Physics, University of Texas, Austin, TX 78712, USA*
[b] *Institute of Theoretical Physics, Chinese Academy of Science, Beijing 100190, P. R. China*
E-mail: elenac@utexas.edu, anderson.misobuchi@utexas.edu, mingleix@itp.ac.cn

Abstract: In this work we explore the effect of rotation in the size of a traversable wormhole obtained via a double trace boundary deformation. We find that at fixed temperature *the size of the wormhole increases with the angular momentum* $J/M\ell$. The amount of information that can be sent through the wormhole increases as well. However, for the type of interaction considered, the wormhole closes as the temperature approaches the extremal limit. We also briefly consider the scenario where the boundary coupling is not spatially homogeneous and show how this is reflected in the wormhole opening.

Contents

1 Introduction

Wormhole solutions to Einstein's equations connect two asymptotically different regions of spacetime. However, they cannot be used to travel form one of the regions to the other since traversable wormholes are forbidden in classical general relativity. Their existence would require a violation of the Average Null Energy Condition (ANEC) usually achieved by including exotic matter. ANEC states that the stress energy tensor integrated along a complete null geodesic is always a positive quantity,

$$\int_\gamma T_{\mu\nu} k^\mu k^\nu d\lambda \geqslant 0, \tag{1.1}$$

where the null vector k^μ is tangent to the geodesic γ and λ is an affine parameter. ANEC plays a crucial role in singularity theorems and it has been proven to hold [1–3] along achronal [1] null geodesics. Null geodesics in Minkowski and in Anti-de Sitter are achronal therefore no violation of ANEC is possible and there are no traversable wormholes in neither of these spacetimes.

In [4] the authors considered the scenario of an eternal black hole with two asymptotically AdS boundaries and proposed a mechanism that evades the assumptions of the theorems forbidding ANEC violation. They showed that, semi-classically, including a deformation that couples both boundaries modifies the causal structure rendering the geodesics chronal and ANEC can be violated without contradicting any known theorem. Choosing an appropriate sign for the coupling we see that this is indeed the case; ANEC is violated and the wormhole becomes traversable. One can check this explicitly by following a ray coming from past infinity and traveling along the horizon. After turning on the boundary coupling this ray does not end up in the singularity but makes it to the other boundary signaling that the wormhole has become traversable. Usually, traversable wormholes imply causal inconsistencies because one can obtain closed time-like curves by boosting one end of the wormhole [5]. The scenario of [4] avoids this problem since coupling both boundaries means that no such boosts are allowed.

The scenario presented in [4] has a holographic interpretation in terms of interactions between two CFTs and yields the first traversable wormhole solution that can be embedded in a quantum theory of gravity. In [6] the authors elaborate on the quantum information implications of [4] and study in detail the traversable wormhole in AdS_2 gravity, the conjectured holographic dual of Sachdev-Ye-Kitaev (SYK) model [7, 8]. They emphasize that the scenario proposed in [4] can be viewed as a quantum teleportation protocol. They also estimate the amount of information that can be sent through the wormhole before the wormhole closes. Other aspects of the quantum information implications of [4] can be found in [9–17].

[1] Recall that achronal geodesics are those that do not contain any points that can be connected by a timelike curve.

The mechanism proposed in [4] is beautifully simple and the result is fascinating. It could provide an explanation of how information can escape from a black hole. However, currently, it does not address the full black hole information paradox since for this mechanism to work the information should be in a very special state, the thermofield double state. There are many issues to be understood before we can apply the traversable wormhole protocol to the black hole information problem. Understanding the details of the traversable wormhole protocol and its quantum information implications in more general scenarios is a first step in that direction.

In this context, a natural question to ask is *how the size of the wormhole and the amount of information transferred change in more general gravity backgrounds.* In this work we consider a rotating eternal black hole in three dimensions (rotating BTZ) and study the traversable wormhole produced by including a double trace deformation at the boundary. For simplicity we first consider a constant boundary coupling. We show that, at fixed temperature, the size of the wormhole opening *increases* with the angular momentum. We establish a bound on information that can be transferred and show that in a rotating background more information can be sent through the wormhole as compared with the non-rotating scenario of [4] and [6]. We show that our results are valid for relevant operators of any conformal dimension ($0 < \Delta < 1$). The increase of the bound is particularly noticeable at higher angular momentum J. We also analyze the extremal limit and find that the wormhole closes as we approach $J = M$. The couplings considered in [4] and [6] were homogeneous in the boundary spatial directions. We briefly consider the effect of taking a coupling with dependence on the x boundary directions and investigate how this affects the wormhole opening.

This paper is organized as follows: in section 2 we review the rotating BTZ geometry and establish our notation. In sections 3 and 4 we explore ANEC violation, the size of the traversable wormhole and the bound on information that can be transferred through it; these sections contain our main results. In section 5 we briefly consider the case of a non-homogeneous coupling. Section 6 contains a summary of our results and interesting future directions.

2 Review of the rotating BTZ geometry

The rotating BTZ black hole [18, 19] is a solution of Einstein gravity in $2+1$ dimensions with negative cosmological constant $\Lambda = -1/\ell^2$ described by the action

$$I = \frac{1}{16\pi G_N} \int d^3x \sqrt{-g}(R + 2\ell^{-2}). \tag{2.1}$$

The solution can be constructed from a quotient of global AdS_3. The metric in $(t,\ r,\ \tilde{x})$ coordinates is,

$$ds^2 = -\frac{(r^2-r_+^2)(r^2-r_-^2)}{\ell^2 r^2}dt^2 + \frac{\ell^2 r^2}{(r^2-r_+^2)(r^2-r_-^2)}dr^2 + r^2\left(d\tilde{x} - \frac{r_+ r_-}{\ell r^2}dt\right)^2,$$
$$\tilde{x} \sim \tilde{x} + 2\pi. \tag{2.2}$$

The inner (Cauchy) horizon is r_- and the outer horizon is r_+. The identification in the angular coordinate $\tilde{x}$ breaks the global $SL(2,\mathbb{R}) \times SL(2,\mathbb{R})$ isometry of AdS_3 down to a $\mathbb{R} \times SO(2)$ subgroup. Without the identification, the solution is simply a portion of AdS_3 with a Rindler horizon for an accelerated observer. Since our interest is the region near the outer horizon, it is convenient to work in the co-rotating frame with the shifted angular coordinate

$$x \equiv \tilde{x} - \Omega_H t, \tag{2.3}$$

where $\Omega_H = \frac{r_-}{\ell r_+}$ is the angular velocity of the outer horizon. With this choice the metric becomes

$$ds^2 = -\frac{(r^2-r_+^2)(r^2-r_-^2)}{\ell^2 r^2}dt^2 + \frac{\ell^2 r^2}{(r^2-r_+^2)(r^2-r_-^2)}dr^2 + r^2\left(\mathcal{N}(r)dt + dx\right)^2,$$
$$\mathcal{N}(r) = \frac{r_-}{2r_+}\frac{r^2-r_+^2}{\ell r^2}, \qquad x \sim x + 2\pi. \tag{2.4}$$

This choice is useful because the off-diagonal terms in the metric vanish at the outer horizon.

The thermodynamic variables are,

$$M = \frac{r_+^2 + r_-^2}{8G_N\ell^2}, \quad J = \frac{r_+ r_-}{4G_N\ell}, \quad S = \frac{\pi r_+}{2G_N}, \quad \kappa = \frac{r_+^2 - r_-^2}{\ell^2 r_+}, \quad \beta = \frac{2\pi}{\kappa}, \tag{2.5}$$

where M is the mass, J is the angular momentum, S is the entropy, and κ is the surface gravity of the outer horizon, related to the temperature of the black hole by $\kappa = 2\pi/\beta = 2\pi T$. The horizon exists provided $M > 0$ and $|J| \leqslant M\ell$. Without loss of generality we can assume that J is positive. The extremal limit, in which the two horizons coincide, corresponds to $|J| = M\ell$. We can also rewrite the inner and outer horizons in terms of M and J

$$r_\pm^2 = \frac{1}{16G_N}\left(M\ell^2 \pm \sqrt{(M\ell^2)^2 - J^2\ell^2}\right). \tag{2.6}$$

The Penrose diagram for the maximal extension of the rotating BTZ black hole is depicted in Fig. 1. In principle, the maximal extension allows to continue to negative values of r^2, but since this introduces closed timelike curves the diagram is truncated

at the surface $r = 0$, which is treated as a singularity (see [20] for a more detailed discussion). Note that we will not concern ourselves with the regions behind the r_- horizon $(3_{++}, 3_{-+}, 3_{+-}, 3_{--})$ since the r_- horizon is unstable [21]. Regions 1_{++} and 1_{+-} correspond to the region outside the horizon $(r_+ < r < \infty)$. Embedding coordinates appropriate for region 1_{++} are given by [21]

$$1_{++}: \begin{cases} X_+ = \left[\left(\frac{r-r_+}{r+r_+}\right)\left(\frac{r+r_-}{r-r_-}\right)^{r_-/r_+}\right]^{\frac{1}{2}} \cosh(\kappa\, t) \\ T_+ = \left[\left(\frac{r-r_+}{r+r_+}\right)\left(\frac{r+r_-}{r-r_-}\right)^{r_-/r_+}\right]^{\frac{1}{2}} \sinh(\kappa\, t) \end{cases}, \quad r_+ < r < \infty. \tag{2.7}$$

We can reach the region 1_{+-} from 1_{++} by performing a imaginary shift in time $t \to t - i\beta/2$. Similarly, regions 2_{++} and 2_{+-} can be reached from 1_{++} shifting time by $-i\beta/4$ and $-3i\beta/4$, respectively[2]. Kruskal coordinates are defined as

$$U = X_+ + T_+, \qquad V = X_+ - T_+. \tag{2.8}$$

This choice of Kruskal coordinates is valid only for $r > r_-$. The metric (2.2) becomes

$$\begin{aligned} ds^2 &= -\Omega^2(r) dU dV + \left(\frac{\mathcal{N}(r) r}{2U\kappa} dU - \frac{\mathcal{N}(r) r}{2V\kappa} dV + r dx\right)^2, \\ \Omega^2(r) &\equiv \frac{(r^2 - r_-^2)(r + r_+)^2}{\kappa^2 r^2 \ell^2} \left(\frac{r - r_-}{r + r_-}\right)^{r_-/r_+}, \end{aligned} \tag{2.9}$$

where $r = r(UV)$ is understood as an implicit function. Note that the coordinate transformation becomes singular when $r_+ = r_-$, so taking the strict limit $r_+ = r_-$ is not possible with this choice of coordinates. For this reason, the extremal limit in our analysis will correspond to approach $r_+ \to r_-$, but still keeping $r_+ \neq r_-$.

3 Opening the wormhole with a double trace deformation

In AdS/CFT the eternal AdS black hole geometry is understood to be dual to two copies of a CFT living in the two asymptotic boundaries (corresponding to regions 1_{++} and 1_{+-} in Fig. 1) in the thermofield double state (TFD) [22],

$$|\Psi\rangle = \frac{1}{\sqrt{Z(\beta, \Omega_H)}} \sum_n e^{-\beta(E_n - \Omega_H J_n)/2} |E_n, J_n\rangle_L |E_n, J_n\rangle_R, \tag{3.1}$$

[2]In the co-rotating frame there is no change in x when we move to other region, but in the original coordinate system $\tilde{x}$ is shifted by $\tilde{x} \to \tilde{x} - i\beta\Omega_H/2$ when we move a point from 1_{++} to 1_{+-}, for example.

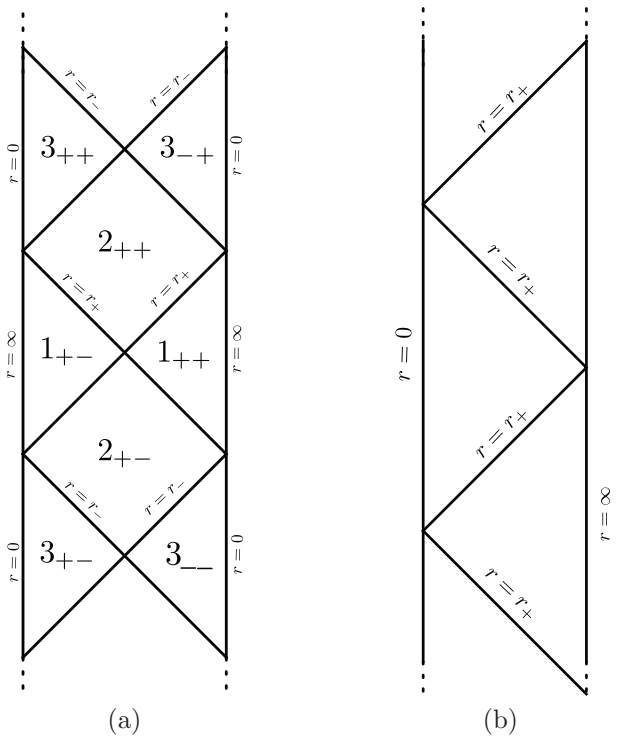

Figure 1: (a) Penrose diagram for maximally extended rotating BTZ (non-extremal). Regions $1_{+\pm}$: $r > r_+$. Regions $2_{+\pm}$: $r_- < r < r_+$. Regions $3_{\pm\pm}$: $r < r_-$. (b) Penrose diagram for the extremal limit $r_+ = r_-$.

where $Z = \mathrm{Tr}\, e^{-\beta(H-\Omega_H J)}$ is the partition function. The sum runs over a complete basis of eigenstates with energy E_n and angular momentum J_n. We can view the combination $\tilde{H}_{L/R} = H_{L/R} - \Omega_H J_{L/R}$ as the effective Hamiltonian that evolves the Left/Right system. When we consider the evolution for the full system defined in the Hilbert space $\mathcal{H} = \mathcal{H}_L \otimes \mathcal{H}_R$ there are two possibilities for the choice of sign for the Hamiltonian. Here we choose the combination $\tilde{H}_R - \tilde{H}_L$ which leaves the TFD invariant.

In the identification of the eternal rotating BTZ with the TFD state, it is implicitly assumed that the dual theory is defined in the two boundaries in regions 1_{++} and 1_{+-} instead of the infinite disconnected boundaries present in the maximal extension [23, 24]. Moreover, as previously mentioned, the region behind the r_- horizon is excluded since it is known that scalar perturbations lead to instabilities of the Cauchy horizon. In our work the focus is in the region close to the outer horizon so this subtlety plays no role in our analysis.

Gao, Jafferis and Wall (GJW) [4] showed that a wormhole in the eternal AdS black hole scenario can be made traversable by turning on a coupling between the

left and right boundaries of form

$$\delta H(t_1) = -\int d^{d-1}x_1\, h(t_1, x_1)\mathcal{O}_R(t_1, x_1)\mathcal{O}_L(-t_1, x_1), \tag{3.2}$$

where for simplicity we choose,

$$h(t_1, x_1) = \begin{cases} h\kappa^{2-2\Delta}, & t_0 \leqslant t_1 \leqslant t_f \\ 0 \qquad\quad , & \text{otherwise.} \end{cases} \tag{3.3}$$

$\mathcal{O}_{L/R}$ is a scalar operator of dimension[3] $\Delta = \frac{d}{2} - \sqrt{\left(\frac{d}{2}\right)^2 + m^2}$ living in the Left/Right CFT, dual to a bulk scalar field Φ with mass m. For a suitable choice of the sign of the coupling this interaction produces negative null energy in the bulk violating the Averaged Null Energy Condition (ANEC). Using the linearized Einstein equations we will show in Sec. 3.2 that the effect of the interaction is to produce a negative shift ΔV, so that a test particle sent from one boundary traveling near the horizon can reach the other side.

3.1 Bulk-to-boundary propagator in a rotating background

One key ingredient to study traversability is the knowledge of the bulk-to-boundary propagator. Since the rotating BTZ solution is locally AdS_3, the bulk-to-boundary propagator can be obtained from the propagator for AdS_3 via a coordinate transformation. The result when both bulk and boundary points are contained in region 1_{++} is [21],

$$\mathcal{K}(z, t, x; t_1, x_1) = \\ \frac{(r_+^2 - r_-^2)^{\frac{\Delta}{2}}}{2^{\Delta+1}\pi\ell} \sum_{n=-\infty}^{\infty} \left[-\sqrt{z-1}\cosh\left(\kappa\delta t - \frac{r_-}{\ell}\delta x_n\right) + \sqrt{z}\cosh\left(\frac{r_+}{\ell}\delta x_n\right)\right]^{-\Delta}, \tag{3.4}$$

where

$$z = \frac{r^2 - r_-^2}{r_+^2 - r_-^2}, \quad \delta t = t - t_1, \quad \text{and} \quad \delta x_n = x - x_1 + 2\pi n. \tag{3.5}$$

Note that the overall normalization of the propagator is obtained by taking the limit to the boundary from the bulk-to-bulk propagator [25, 26], such that it agrees with the propagator considered by GJW in the limit $r_- \to 0$. Near the event horizon in the region 1_{++}, it is possible to explicitly invert the Kruskal coordinates (2.8) to obtain

$$t = \frac{1}{2\kappa}\log\left(-\frac{U}{V}\right), \qquad z = 1 - \gamma^2\, UV + O(U^2V^2), \tag{3.6}$$

[3] In principle there are two choices of sign $\Delta_\pm = \frac{d}{2} \pm \sqrt{\left(\frac{d}{2}\right)^2 + m^2}$, but we pick the minus sign to have a relevant deformation, which constrains $0 < \Delta < 1$ for $d = 2$.

where we have defined

$$\gamma^2 \equiv \Omega^2(r=r_+) = \frac{4r_+^2\ell^2}{r_+^2-r_-^2}\left(\frac{r_+-r_-}{r_++r_-}\right)^{r_-/r_+}. \tag{3.7}$$

For example, the bulk-to-boundary propagator along $V=0$ for both points contained in region 1_{++} becomes (omiting sum over images)

$$\mathcal{K}(U,0,x;\,U_1,x_1) = \frac{\left(r_+^2-r_-^2\right)^{\frac{\Delta}{2}}}{2^{\Delta+1}\pi\ell}\left(\frac{1}{-\frac{\gamma}{2}U/U_1 e^{-r_-(x-x_1)}+\cosh[r_+(x-x_1)]}\right)^{\Delta}, \tag{3.8}$$

and propagators for points in different regions can be obtained using the imaginary shifts in time that we have described in Sec. 2. We will also need the retarded bulk-to-boundary propagator, which can be expressed as

$$\begin{aligned}&\mathcal{K}_{\rm ret}(z,t,x;t_1,x_1) = \\ &= |\mathcal{K}(z,t,x;t_1,x_1)|\,\theta(\delta t)\,\theta\left(\sqrt{z-1}\cosh\left(\kappa\,\delta t-\frac{r_-}{\ell}\delta x\right)-\sqrt{z}\cosh\left(\frac{r_+}{\ell}\delta x\right)\right).\end{aligned} \tag{3.9}$$

Throughout the rest of the paper we will set $\ell=1$ for simplicity.

3.2 ANEC violation and wormhole size

We now evaluate the modified stress tensor in the rotating BTZ background when we turn on the interaction (3.2). The analytic continuation of the bulk-to-boundary propagator when the points are time-like separated from the boundary was studied in [24]. This continuation works very much like in the non-rotating case. Therefore, the steps of the calculation follow closely [4].

The starting point is to evaluate the bulk two-point function

$$G(U,U') \equiv \langle \Phi_R(U,x)\Phi_R(U',x)\rangle. \tag{3.10}$$

In the perturbative expansion in the coupling h, the one-loop contribution to the two-point function is

$$G_h = \frac{2h\sin(\pi\Delta)}{\kappa^{2\Delta-2}}\int_{t_0}^{t_f} dt_1 dx_1 \mathcal{K}(r',t',x';-t_1+i\tfrac{\beta}{2},x_1)\mathcal{K}_{\rm ret}(r,t,x;t_1,x_1)+(t\leftrightarrow t'), \tag{3.11}$$

where we used the imaginary shift $t\to t-i\beta/2$ to move all the points to the right region 1_{++}. Using the propagators (3.4) and (3.9), and evaluating at $V=0$ in

Kruskal coordinates gives

$$G_h(U,U') = C_0 \int_{U_0}^{U} \frac{dU_1}{U_1} \left(\frac{1}{\frac{\gamma}{2} e^{-r_- \delta x} U_1 U' + \cosh(r_+ \delta x)} \right)^{\Delta} \left(\frac{U_1}{\frac{\gamma}{2} e^{-r_- \delta x} U - U_1 \cosh(r_+ \delta x)} \right)^{\Delta} dx_1 + (U \leftrightarrow U') \tag{3.12}$$

where $U_0 = e^{\kappa t_0}$. After we shut down the interaction ($U > U_f = e^{\kappa t_f}$) the upper limit in the U_1 integral should be replaced by U_f. The overall constant is

$$C_0 = \frac{h \kappa^{1-\Delta} r_+^{\Delta} \sin(\Delta\pi)}{2(2^{\Delta}\pi)^2}. \tag{3.13}$$

The sum over the images extends the domain of the x_1 integral to the entire real axis, but it ends being constrained by the $\theta-$function in the retarded propagator (3.9), which requires that

$$\frac{\gamma}{2}\, e^{-r_- \delta x} U - U_1 \cosh(r_+ \delta x) \geqslant 0. \tag{3.14}$$

The bulk stress tensor associated to the scalar field Φ is

$$T_{\mu\nu} = \partial_\mu \Phi \partial_\nu \Phi - \frac{1}{2} g_{\mu\nu} g^{\rho\sigma} \partial_\rho \Phi \partial_\sigma \Phi - \frac{1}{2} g_{\mu\nu} m^2 \Phi^2. \tag{3.15}$$

At one-loop, the expectation value of the stress tensor for the perturbed Hamiltonian can be evaluated via point splitting

$$\langle T_{\mu\nu} \rangle = \lim_{\mathrm{x} \to \mathrm{x}'} \left(\partial_\mu \partial_\nu G(\mathrm{x},\mathrm{x}') - \frac{1}{2} g_{\mu\nu} g^{\rho\sigma} \partial_\rho \partial_\sigma G(\mathrm{x},\mathrm{x}') - \frac{1}{2} g_{\mu\nu} m^2 G(\mathrm{x},\mathrm{x}') \right). \tag{3.16}$$

When evaluated along the horizon at $V = 0$, the g_{UU} component of the unperturbed metric vanishes, so the leading contribution to the null component of the stress tensor is,

$$T_{UU} = \lim_{U' \to U} \partial_U \partial_{U'} G_h(U,U'). \tag{3.17}$$

where the perturbed propagator $G_h(U,U')$, obtained in (3.12), can be evaluated numerically. Evaluating (3.17) we can find the effect of the double trace deformation on the average null energy. As we see in Fig. 2 our results show that the ANEC is violated.

As mentioned in Sec. 1, ANEC violation is a necessary condition for a wormhole becoming traversable. It is illuminating to explicitly follow a null ray in the perturbed metric going from past infinity ($U \to -\infty$) to future infinity ($U \to \infty$) along the $V = 0$ horizon. The linearized Einstein equation for the UU component for the fluctuations

evaluated at $V = 0$ gives

$$\int dU \left(\frac{\kappa}{2r_+} h_{UU} - \frac{r_- \partial_x h_{UU}}{r_+^2} - \frac{\partial_x^2 h_{UU}}{2r_+^2} \right) = 8\pi G_N \int dU T_{UU}, \tag{3.18}$$

where we assume that the fluctuations vanish at infinity. Since the interaction (3.2) is being integrated over the transverse space, the modified stress tensor should be independent of the transverse coordinate x. This reduces the equation to

$$8\pi G_N \int dU T_{UU} = \frac{\kappa}{2r_+} \int dU h_{UU} = \frac{r_+^2 - r_-^2}{2r_+^2} \int dU h_{UU}. \tag{3.19}$$

We can now relate the average null energy to the shift $\Delta V(U)$ in the null geodesics at the horizon caused by the interaction. After including the perturbation, we can see from the metric (2.9) that the null ray originating in the past is given by,

$$\Delta V(U) = -\frac{1}{2g_{UV}(0)} \int_{-\infty}^{U} dU h_{UU} \tag{3.20}$$

where $g_{UV}(0)$ is the UV component of the original metric evaluated on $V = 0$. Now, from (3.19) and (3.20) we get,

$$\Delta V(U) = \frac{1}{2} \left(\frac{r_+ - r_-}{r_+ + r_-} \right)^{-\frac{r_-}{r_+}} 8\pi G_N \int_{-\infty}^{U} dU T_{UU}. \tag{3.21}$$

We identify the "size" of opening of the wormhole as $\Delta V(\infty)$, which we will denote simply by ΔV.

3.2.1 Numerical results

In our numerical analysis we have set $h = 1$, $G_N = 1$, and the interaction was turned on between $t_0 = 0$ and $t_f = 1$. Fig. 2 shows the ANE obtained by evaluating (3.17) numerically at fixed temperatures as a function of the dimensionless ratio J/M. Note that the curves never reach the value $J/M = 1$ since we are fixing a non-zero temperature (non-extremal case). We see that the ANEC is violated and this violation is more pronounced for increasing temperatures. As a check of our numerical results, note that the red (solid) curve in Fig. 2 corresponds to the same temperature chosen in [4] and the value for $J = 0$ in our plot coincides with the numerical value they obtained for $\Delta = 0.6$.

One of the motivations of this work is to find out if the traversable wormhole is larger in a rotating background. We find that the answer is positive for $h > 0$. *The wormhole opening becomes larger as we increase* J/M; see Fig. 3. This increasing is mainly due to the geometrical factor in (3.21) relating the opening of the wormhole

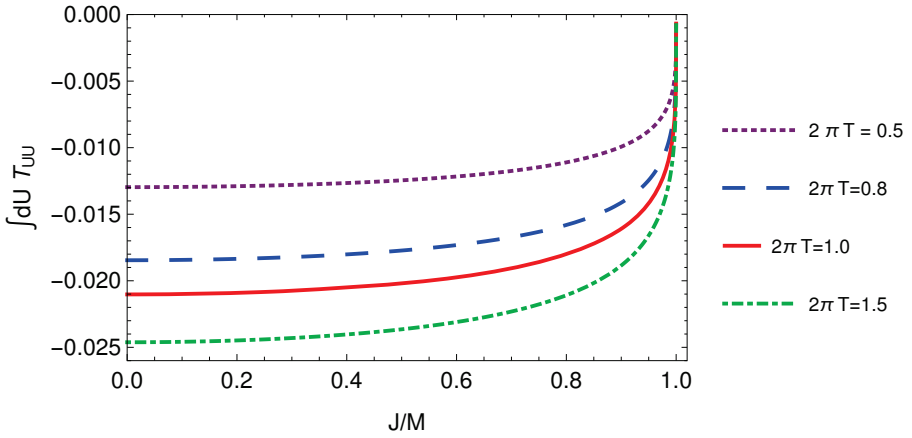

Figure 2: Average null energy at fixed temperatures as a function of angular momentum. We have set $\Delta = 0.6$.

and the ANE. In the next section we will re-derive this result using the out-of-time order correlators approach developed in [6].

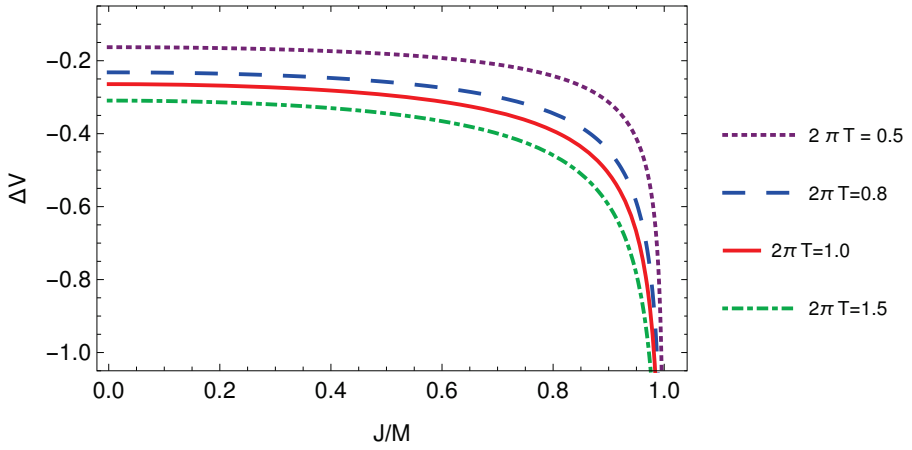

Figure 3: Size of the opening of the wormhole as a function of angular momentum. We have set $\Delta = 0.6$.

So far we have only considered the case of fixed temperatures that does not give us much information about the extremal limit, in which $T \to 0$ and $J \to M$. We can investigate the extremal limit by keeping the mass fixed and varying J and T simultaneously. Our results show that the wormhole closes as we approach the extremal limit; see Fig. 4a. We note that the variation in the opening near the extremal limit is very abrupt if we take the limit with fixed mass. We have also plotted the opening by fixing r_+, which corresponds to fix the black hole entropy, as a function of the angular velocity $\Omega_H = \frac{r_-}{r_+}$; see Fig. 4b.

The numerical results presented in Fig. 2-4 were obtained for boundary operators of conformal dimension $\Delta = 0.6$. We repeat the calculation for different values of Δ

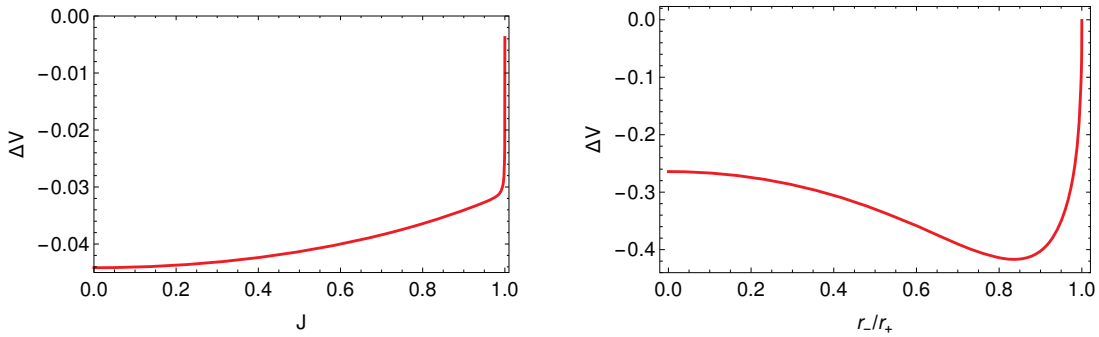

(a) Fixed $M = 1$. (b) Fixed $r_+ = 1$.

Figure 4: Opening of the wormhole with temperature not fixed. The wormhole closes as we approach the extremal limit. We have set $\Delta = 0.6$.

and we find that for any value of allowed conformal dimension $(0 < \Delta < 1)$ there is a violation of ANEC implying a traversable wormhole; see Fig. 5-6.

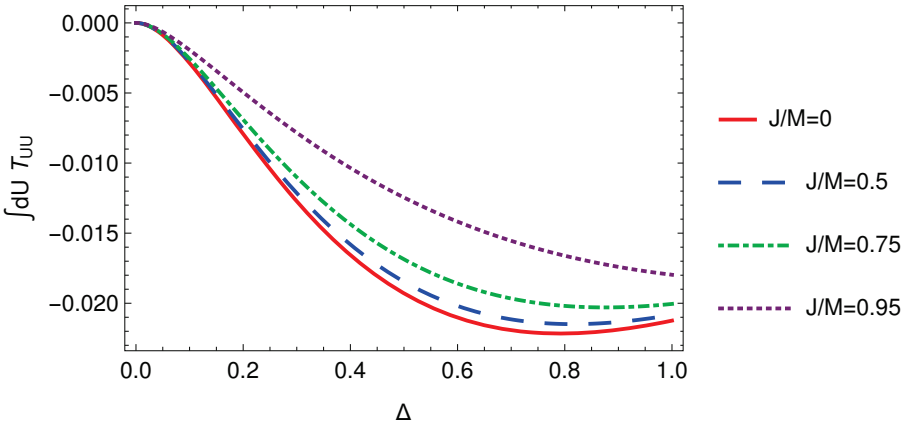

Figure 5: Average null energy for different values of the conformal dimension Δ at fixed temperature $T = \frac{1}{2\pi}$.

4 Bound on information transfer and backreaction

4.1 Diagnose of traversability from Left/Right commutator

In [6] the authors elaborated on the quantum information interpretation of the results in [4]. Focusing on nearly AdS_2 gravity [27], which is claimed to be the dual of the SYK model, they presented a bound on the information that can be transferred through the wormhole. They also considered a double trace deformation[4] but

[4]More precisely, they considered the slightly different interaction $\frac{g}{K}\sum_{j=1}^{K}\mathcal{O}_R^j(0)\mathcal{O}_L^j(0)$, where the K fields are introduced to make the effect larger and the interaction is turned on only at time $t = 0$.

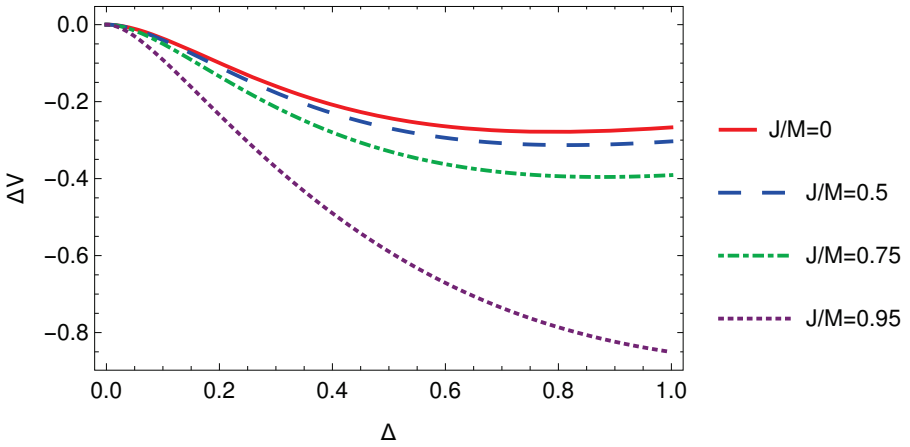

Figure 6: Wormhole opening for different values of the conformal dimension Δ at fixed temperature $T = \frac{1}{2\pi}$.

proposed a different way to diagnose traversability of the wormhole using techniques involving out-of-time order correlation functions that appear in the context of quantum chaos [28, 29]. In this perspective, traversability can be interpreted as the result of a high energy scattering where the signal particle ϕ scatters with $\mathcal{O}$ and suffers a time advance for positive h, so it can emerge on the other boundary (Fig. 7).

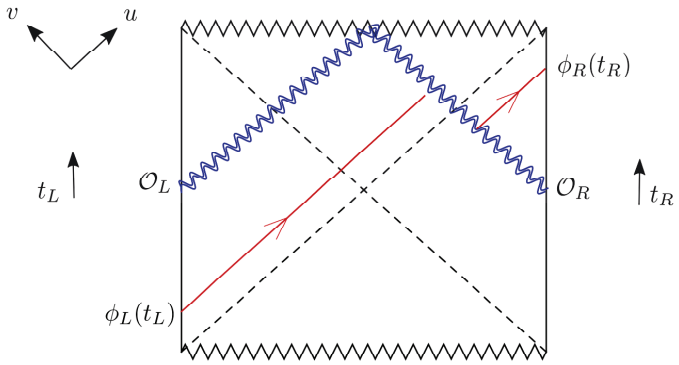

Figure 7: The setup of the traversable wormhole [6]. The double trace deformation produces negative null energy that causes a time advance in the probe ϕ.

In this section we review the diagnose of [6] and we adapt their results to derive the opening of the wormhole for the eternal rotating BTZ black hole. We consider a generic metric in Kruskal coordinates written as

$$ds^2 = -a(uv)dudv + \left(b(u,v)du + c(u,v)dv + r(uv)dx\right)^2, \tag{4.1}$$

and let us define the following quantities evaluated at the horizon

$$a_0 = a(0), \quad r_0 = r(0). \tag{4.2}$$

We will assume that $b(v=0)=0$ to simplify the calculation. Note that this applies to the rotating BTZ case (2.9). In the framework of [6] the diagnose of traversability is based on the commutator

$$\left\langle \left[\phi_L, e^{-i\mathcal{V}}\phi_R\, e^{i\mathcal{V}}\right]\right\rangle, \qquad \mathcal{V}\equiv\int_{t_0}^{t} dt_1\,\delta H(t_1), \tag{4.3}$$

where $\phi_R=\phi_R(t_R)$, $\phi_L=\phi_L(t_L)$, and the brackets $\langle ...\rangle$ denote the expectation value in the TFD state. The convention for time is $t_R=-t_L=t$. If the commutator is non-zero, then the signal from the left boundary successfully reached the right boundary.

Assuming the operators are Hermitian, we can focus on a simpler quantity

$$C\equiv\left\langle e^{-i\mathcal{V}}\phi_R\, e^{i\mathcal{V}}\phi_L\right\rangle, \tag{4.4}$$

which is related to the original commutator via

$$\left\langle \left[\phi_L, e^{-i\mathcal{V}}\phi_R\, e^{i\mathcal{V}}\right]\right\rangle = -2\,\mathrm{Im}(C). \tag{4.5}$$

In the small G_N limit, and assuming the relative boost between $\mathcal{O}$ and ϕ is large, we can approximate the scattering between states created by ϕ and $\mathcal{O}$ by a shock wave with amplitude $S_{\rm grav}=e^{i\tilde{\delta}}$ [30, 31]. The final expression is [6] (see also [13])

$$C=e^{i\langle\mathcal{V}\rangle}\alpha\int dp^u\,dy\,p^u\Psi^*_{\phi_L}(p^u,y)\Psi_{\phi_R}(p^u,y)\,e^{i\mathcal{D}}, \tag{4.6}$$

where $\alpha=\frac{a_0^2 r_0}{4\pi}$. The exponent is defined by

$$\mathcal{D}\equiv\alpha\int dq^v\,dx\int dt_1\,dx_1\,q^v e^{i\tilde{\delta}}h(t_1,x_1)\Psi^*_{\mathcal{O}_R}(q^v,x)\Psi_{\mathcal{O}_L}(q^v,x), \tag{4.7}$$

where the wavefunctions are given by the Fourier transform of the bulk-to-boundary propagators

$$\begin{aligned}
\Psi_{\mathcal{O}_R}(q^v,x)&=\int dv e^{ia_0 q^v v/2}\left\langle\Phi(u,v,x)\,\mathcal{O}^\dagger_R(t_1,x_1)\right\rangle_{u=0},\\
\Psi_{\mathcal{O}_L}(q^v,x)&=\int dv e^{ia_0 q^v v/2}\left\langle\Phi(u,v,x)\,\mathcal{O}_L(-t_1,x_1)\right\rangle_{u=0},\\
\Psi_{\phi_R}(p^u,y)&=\int du e^{ia_0 p^u u/2}\left\langle\Phi_\phi(u,v,y)\,\phi_R(t,y_1)\right\rangle_{v=0},\\
\Psi_{\phi_L}(p^u,y)&=\int du e^{ia_0 p^u u/2}\left\langle\Phi_\phi(u,v,y)\,\phi^\dagger_L(-t,y_1)\right\rangle_{v=0},
\end{aligned} \tag{4.8}$$

and Φ_ϕ is the bulk field dual to ϕ. In the above expression, we have decomposed the

single particle wavefunction of ϕ into states with momentum p^u on the $v = 0$ slice, and momentum q^v on the $u = 0$ slice for $\mathcal{O}$. The operator $\mathcal{O}_{L/R}$ is applied at a point x_1 and $\phi_{L/R}$ is applied at y_1 in transverse space, while x and y are bulk transverse coordinates that appear in the bulk-to-boundary propagators being integrated.

4.2 Probe limit

Here we derive the opening of the wormhole for rotating BTZ using the formula (4.6) in the probe limit. The first step is to derive the scattering amplitude $e^{i\tilde{\delta}}$, which can be found by studying particles propagating along the horizon whose effect is to produce a shock wave geometry [29]. For simplicity, let us assume the matter creating the shock wave is symmetrically distributed over the transverse space, so that the scattering amplitude will be independent of the transverse coordinates.

The parameters (4.2) for the rotating BTZ metric (2.9) are identified as

$$a_0 = \gamma^2, \qquad r_0 = r_+, \tag{4.9}$$

with γ defined as in (3.7). If we send the matter with momentum p_v along $v = 0$, this corresponds to a stress tensor[5]

$$T_{vv} = \frac{-p_v}{r_+ L}\delta(v), \quad \text{so that} \quad -p_v = \int r_+ dx\, dv T_{vv}, \tag{4.10}$$

where L denotes the integral of the transverse coordinate without the measure factor r_+. For rotating BTZ we have $L = 2\pi$, but we keep this factor general to make the dependence on the volume of the transverse space explicit. From the linearized Einstein equations (3.19) for the vv component, we have

$$8\pi G_N T_{vv} = \frac{\kappa}{2r_+} h_{vv}, \tag{4.11}$$

which gives

$$h_{vv} = a_0 a^u \delta(v), \quad a^u \equiv -\frac{16\pi G_N}{a_0 \kappa L} p_v. \tag{4.12}$$

The effect is then to produce a translation by an amount a^u once we cross the horizon $v = 0$. Note that $a^u > 0$ since p_v is negative for a physical particle. The scattering amplitude is identified as

$$i\tilde{\delta} = -i a^u q_u. \tag{4.13}$$

In the probe limit, in which we assume a^u is small, we can expand the exponent in (4.7) for small a^u. The zeroth order term of the expansion cancels with $e^{i\langle\mathcal{V}\rangle}$ in the expression for C (4.6), while the term proportional to a^u contributes to a term that acts as a translation for the ϕ wavefunction. In the end we obtain a correlator

[5]Upper and lower indices are related by $q^v = -\frac{2}{a_0} q_u$, $p^u = -\frac{2}{a_0} p_v$.

for ϕ that has the form

$$C_{\text{probe}} = \left\langle \phi_R e^{-ia^v \hat{P}_v} \phi_L \right\rangle, \tag{4.14}$$

where

$$a^v = -\frac{i\alpha}{p^u} \int dq^v\, dx \int dt_1\, dx_1\, q^v\, \tilde{\delta}\, h(t_1, x_1) \Psi^*_{\mathcal{O}_R}(q^v, x) \Psi_{\mathcal{O}_L}(q^v, x), \tag{4.15}$$

and $\hat{P}_v$ is the translation operator that shifts the ϕ_L wavefunction by an amount a^v along the v direction. This gives us the opening of the wormhole in the probe limit that was calculated using a different method in Sec. 3.2. The quantity a^v here corresponds to ΔV in (3.21).

Let us evaluate (4.15) for the rotating BTZ. The wavefunctions $\Psi_{\mathcal{O}_{L/R}}$ can be computed explicitly since we know the form of the bulk-to-boundary propagator, which evaluated at $u = 0$ is

$$\mathcal{K}(0, v, x; t_1, x_1) = \frac{\left(r_+^2 - r_-^2\right)^{\frac{\Delta}{2}}}{2^{\Delta+1}\pi} \left(\frac{1}{-v\frac{\gamma}{2} e^{-r_-(x-x_1)} e^{-\kappa t_1} + \cosh[r_+(x-x_1)]} \right)^{\Delta}. \tag{4.16}$$

By performing the Fourier transform we obtain the wavefunctions

$$\begin{aligned} \Psi_{\mathcal{O}_L}(q^v, x) &= \tfrac{2^{1+\Delta} q^v (q^v\gamma)^{-2+\Delta} (r_+\kappa)^{\Delta/2}}{\Gamma(\Delta)} e^{i\cosh[r_+(x-x_1)] e^{-r_-(x-x_1)\kappa t_1} q^v \gamma - \frac{i\pi\Delta}{2} - r_-\Delta(x-x_1) + \kappa t_1}, \\ \Psi^*_{\mathcal{O}_R}(q^v, x) &= \Psi_{\mathcal{O}_L}(q^v, x)|_{t_1 \to -t_1}. \end{aligned} \tag{4.17}$$

We can evaluate (4.15) by performing the integral over q^v first. The integral over x_1 is extended over all real axis because we are summing over the contribution of all images coming from the periodicity in the transverse coordinate. At the end we obtain

$$a^v = -\frac{h\, G_N\, 4^{1-2\Delta} r_+^{1+\Delta} \kappa^{1-\Delta} \Gamma(1+2\Delta)}{\gamma\, \Gamma(\Delta)} I_{t_1} I_{x_1}, \tag{4.18}$$

where the integrals I_{t_1} and I_{x_1} can be evaluated in terms of beta and hypergeometric functions

$$I_{t_1} = \int_{t_0}^{t_f} \frac{dt_1}{\cosh^{1+2\Delta}(\kappa\, t_1)} = \frac{i}{2\kappa} \left[B(\cosh^2(\kappa\, t_f), -\Delta, \tfrac{1}{2}) - B(\cosh^2(\kappa\, t_0), -\Delta, \tfrac{1}{2}) \right], \tag{4.19}$$

$$\begin{aligned} I_{x_1} &= \int_{-\infty}^{\infty} \frac{dx\, e^{r_-(x-x_1)}}{\cosh^{1+2\Delta}[r_+(x-x_1)]} \\ &= 2^{1+2\Delta} \left[\frac{{}_2F_1\left(\frac{r_+ + r_-}{2r_+} + \Delta, 1+2\Delta, \frac{3}{2} + \frac{r_-}{2r_+} + \Delta, -1\right)}{r_+(1+2\Delta) + r_-} + \frac{{}_2F_1\left(\frac{r_+ - r_-}{2r_+} + \Delta, 1+2\Delta, \frac{3}{2} - \frac{r_-}{2r_+} + \Delta, -1\right)}{r_+(1+2\Delta) - r_-} \right]. \end{aligned} \tag{4.20}$$

This tells us that the ϕ_L signal, in the probe limit, is shifted by an amount a^v in the

v direction. If we choose h to be positive, then a^v is negative and the wormhole is traversable. The result for the opening agrees with the numerical calculation using the method of [4] discussed in Sec. 3.2.

4.3 Bound from probe limit

In the probe limit we have assumed that the typical momentum of the state created by ϕ is small. Once we increase the momentum, the wormhole starts to close and therefore a bound on the information transferred is expected. In this section, following [6], and using the opening in probe limit obtained in Sec. 4.2, we find a bound on the information that can be transferred through the wormhole. In the next section we present a refined version of the bound using a more careful treatment of the backreaction effects.

Let us assume that we are sending many particles with same characteristic momentum p_v. Effectively, this corresponds to treat the wavefunctions $\Psi_{\phi_{L/R}}$ in (4.6) as multiparticle wavefunctions, and replace the momentum that appear in the scattering amplitude (4.13) by the total momentum $p_v^{\text{total}} = \sum_l p_v^l$, where l is an index for each individual particle. The amount of information N_{send} sent through the wormhole can be defined via

$$N_{\text{send}} \equiv \frac{p_v^{\text{total}}}{p_v}. \tag{4.21}$$

Using the uncertainty principle $p_v\, a^v \gtrsim 1$, we obtain[6]

$$N_{\text{send}} \lesssim a^v p_v^{\text{total}}. \tag{4.22}$$

The validity of the probe approximation breaks down when the scattering amplitude $\tilde{\delta}$ becomes order one, so we will require that $\tilde{\delta} \lesssim 1$. Using (4.13) we obtain

$$N_{\text{send}} \lesssim \frac{|a^v| L \gamma^2 \kappa}{16\pi G_N q_u}, \tag{4.23}$$

where q_u in the above expression corresponds to the characteristic value of momenta for the particles created by $\mathcal{O}$.

In the case of AdS_2 studied in [6], the resulting bound (up to an order one constant) was simply given by the value of the coupling. The same happens in our case since the opening of the wormhole a^v is proportional to h. The physical interpretation of the bound (4.23) becomes more evident by making use of the linearized

[6] A more rigorous derivation using monotonicity of relative entropy instead of the uncertainty principle was also presented in [6] using an argument from [32], resulting in the same inequality up to a factor of 2π.

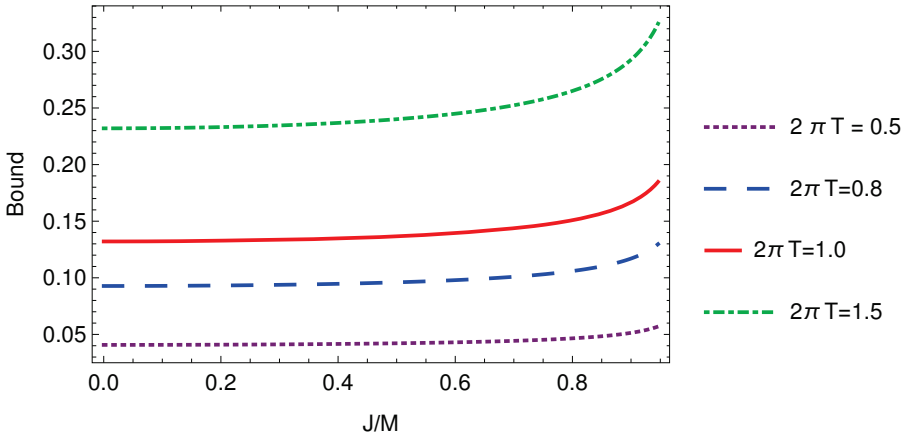

Figure 8: Bound on N_{send} using Eq. (4.23), assuming momentum is sent spherically over transverse space at fixed temperatures. We fixed $h = 1$, $\Delta = 0.6$, $t_0 = 0$, $t_f = 1$.

Einstein equations (3.19) allowing us to express the bound in terms of the ANE

$$N_{\text{send}} \lesssim \frac{r_+ L \left| \int du T_{uu} \right|}{q_u}. \tag{4.24}$$

If we assume that the characteristic momenta q_u is order one, we conclude that the bound on information is simply given by the ANE multiplied by the volume of the transverse space.

There is still an order one constant ambiguity in the above bound. However, the bound still captures the dependence on the temperature and the angular momentum since we carried the dependence on the r_+ and r_- parameters in all steps. Fig. 8 shows that the bound becomes larger as we increase the dimensionless ratio J/M at fixed temperatures. By looking at (4.24) and from our result for the ANE obtained in Sec. 3.2.1, we see that this increase is mostly due to a respective increase in the r_+ parameter, which is equivalent to an increase in the black hole entropy (2.5).

In Fig. 9, we show the behavior of the bound as we vary both J and T. In particular, as we approach the extremal limit, the bound on information goes to zero, which is consistent with our result in Sec. 3.2.1 where the wormhole closes in the extremal limit. The closing of the wormhole is somewhat expected since the wormhole throat becomes infinitely long at extremality [33, 34]. We note, however, that the traversable wormhole presented here depends on several parameters in the interaction profile (3.2) such as the time interval in which the interaction is turned on. It is plausible that scaling the parameters one can obtain a non-zero opening size even in the extremal limit. Indeed, an example of a traversable wormhole at extremality was recently found in [35] by incorporating the backreaction of quantum fields with adequate boundary conditions.

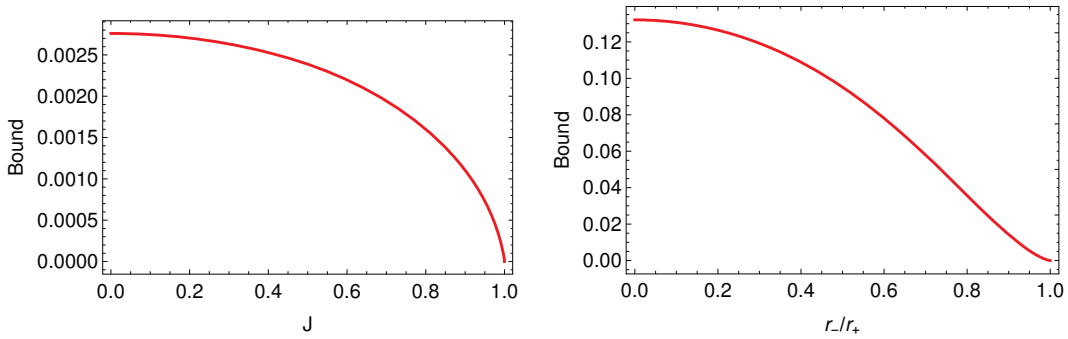

(a) Fixed $M = 1$. (b) Fixed $r_+ = 1$.

Figure 9: Bound on information transfer.

4.4 Improving analysis with backreaction

Even though the insertion of the operator ϕ contributes only to the T_{vv} component of the stress tensor, the ANE along $v = 0$ evaluated from (3.17) still gets modified once we include the backreaction of ϕ. This can be understood as ϕ producing a shock wave localized along $v = 0$, which delays the quanta produced by $\mathcal{O}_R$; Fig. 10. As a result, the effect of the double trace interaction becomes weaker, decreasing the ANE injected into the bulk and closing the wormhole.

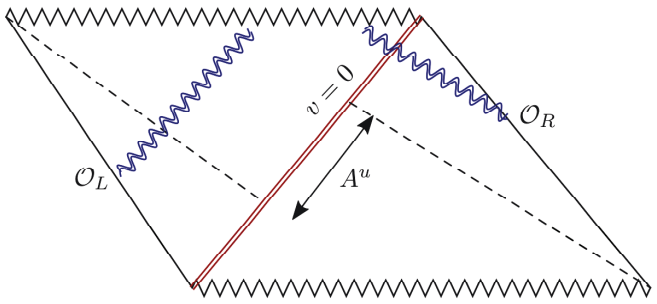

Figure 10: The backreaction of ϕ produces a shock wave geometry. The wavefunction associated to $\mathcal{O}_R$ suffers a time delay when it crosses the horizon at $v = 0$.

Here, we investigate the effect of backreaction in the opening of the wormhole by applying the double trace deformation in the BTZ geometry perturbed by the shock wave produced by ϕ. This can be accomplished simply by replacing $U' \to U' + A^u$ in (3.12), which corresponds to apply a shift in the U direction to the bulk-to-boundary propagator that originally connected the left boundary to a point at the horizon. The parameter A^u is related to the total momentum sent through the wormhole via

$$A^u = -\frac{16\pi G_N}{a_0 \kappa L} p_v^{\text{total}}. \tag{4.25}$$

Alternatively, using the diagnose of traversability of [6], we can apply a translation in the wavefunction $\Psi_{\mathcal{O}_R}$

$$\Psi_{\mathcal{O}_R} \to e^{-iA^u q_u} \Psi_{\mathcal{O}_R}. \tag{4.26}$$

For the purpose of the calculation, we can imagine that we send an extra particle with momentum $p_v \ll p_v^{\text{total}}$. We can then treat this particle as a probe for the opening of the wormhole that will now depend on p_v^{total}. In this picture the effective scattering amplitude becomes

$$i\delta_{\text{total}} = -i(A^u + a^u)q_u \tag{4.27}$$

where

$$a^u = -\frac{16\pi G_N}{a_0 \kappa L} p_v. \tag{4.28}$$

We can expand in a^u to linear order, so that the particle with momentum p_v will acquire a shift in the v direction, which we identify as the opening of the wormhole including the backreaction. The integral over q^v for the exponent of (4.6) gives

$$\mathcal{D} = \mathcal{D}_0 \int dt_1 dx_1 dx \left(\frac{e^{r_-(x-x_1)}}{\gamma(A^u + a^u) + 4e^{-r_-(x-x_1)} \cosh[r_+(x-x_1)] \cosh(\kappa t_1)} \right)^{2\Delta}, \tag{4.29}$$

where the coefficient $\mathcal{D}_0$ is

$$\mathcal{D}_0 = \frac{h r_+^{1+\Delta} \kappa^{2-\Delta} \Gamma(2\Delta)}{\pi \Gamma(\Delta)^2}. \tag{4.30}$$

After expanding to first order in a^u we obtain wormhole opening,

$$a^v_{\text{back}} = \mathcal{A}_0 \int \frac{dx\, dt_1\, e^{r_-(x-x_1)}}{(4\pi G_N e^{r_-(x-x_1)}(-p_v^{\text{total}}/L) + \gamma\kappa \cosh(r_+(x-x_1)) \cosh(\kappa t_1))^{1+2\Delta}}, \tag{4.31}$$

where $\mathcal{A}_0$ is,

$$\mathcal{A}_0 = -4^{1-2\Delta} h G_N \gamma^{2\Delta} r_+^{1+\Delta} \kappa^{2+\Delta} \frac{\Gamma(1+2\Delta)}{\Gamma(\Delta)^2}. \tag{4.32}$$

Evaluating (4.31) numerically we obtain the opening of the wormhole with backreaction; see Fig. 11. Our parameters were fixed as $h = 1$, $G_N = 1$, $\Delta = 0.6$, $t_0 = 0$, $t_f = 1$, and $T = \frac{1}{2\pi}$. We see that the wormhole closes as we increase the momentum p_v^{total} sent through it.

We can obtain a refined bound by determining the momentum that maximizes the right hand side of (4.22),

$$N_{\text{send}} \lesssim \max\left[a^v_{\text{back}}\, p_v^{\text{total}}\right], \tag{4.33}$$

which corresponds to determine the maximum values in the curves displayed in Fig 12. This improves the bound by removing the order one ambiguity in the step in

which we assumed $\tilde{\delta} \lesssim 1$. Comparing with the previous estimative in Fig. 8 at same temperature $T = \frac{1}{2\pi}$, we see that the refined bound is slightly smaller, suggesting a sharper bound.

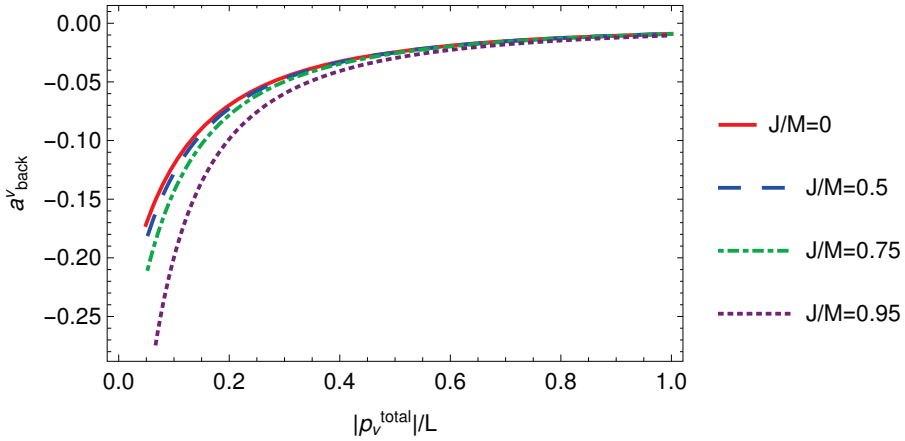

Figure 11: Opening of the wormhole as a function of momentum p_v^{total} sent spherically distributed over transverse space. Fixed temperature $T = \frac{1}{2\pi}$.

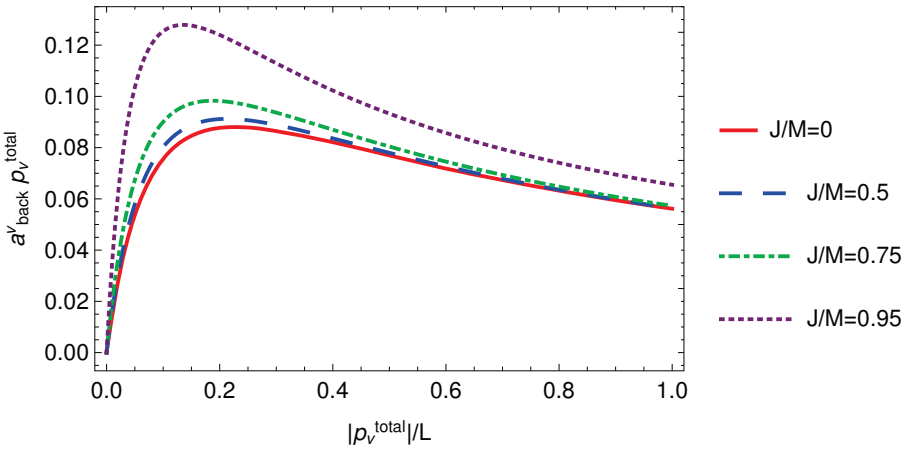

Figure 12: Bound on information given by $N_{\text{send}} \lesssim a^v_{\text{back}}\, p_v^{\text{total}}$ for spherically distributed momentum. Fixed temperature $T = \frac{1}{2\pi}$.

5 Dependence on transverse coordinates

In the previous sections we have considered the double trace interaction (3.2) with a uniform coupling so that the size of the opening of the wormhole was independent of the transverse coordinate x. A natural question to ask is how the opening changes if we consider instead a non-homogeneous coupling. In this section, we briefly analyze this question by deriving the opening of the wormhole in the probe limit by

considering the modified interaction

$$\delta H_{\rm loc}(t_1) = -g\,\mathcal{O}_R(t_1, x_1)\mathcal{O}_L(-t_1, x_1), \tag{5.1}$$

which is turned on only in the direction x_1 in transverse space, for a time $t_0 \leqslant t_1 \leqslant t_f$. We will follow again the approach used in [6]. We can probe the opening of the wormhole by assuming that the momentum p_v produced by the operator ϕ is localized at some position y_1. For the background in the form of (4.1), this contributes to the stress tensor with [29]

$$T_{vv} = \frac{a_0}{2r_0} p^u \delta(y - y_1), \tag{5.2}$$

and the effect is to produce a shock wave localized around y_1

$$h_{vv}(y - y_1) = 8\pi G_N r_+ p^u a_0 \delta(V) f(y - y_1), \tag{5.3}$$

where $f(y)$ is a transverse profile that can be determined from the linearized Einstein equations. Specializing to our rotating geometry the solution is given by

$$f(y) = \frac{e^{r_-\, y - r_+|y|}}{2r_+}, \tag{5.4}$$

which is obtained by solving the equation

$$-f''(y) + 2r_- f'(y) + (r_+^2 - r_-^2) f(y) = \delta(y). \tag{5.5}$$

The corresponding scattering amplitude is

$$\tilde{\delta}_{\rm loc} = \frac{16\pi G_N r_+ p_v f(x)}{a_0} q_u \tag{5.6}$$

Using this scattering amplitude, we can derive the opening of the wormhole using (4.15) again, but now the opening will be a function of the separation $y - x_1$ between ϕ and $\mathcal{O}$ in the transverse space. We plotted the result in Fig. 13. The wormhole opening is peaked near x_1, but due to the presence of rotation the maximum value of the opening is slightly shifted to the right.

6 Conclusions and future directions

In this work we explored the effect of rotation in the size of a traversable wormhole obtained via a double trace boundary deformation. We find that the size of the wormhole and the amount of information that can be transferred through it increases in a rotating geometry. We improved on the existing bound on information transferred by taking into account the backreaction. We also briefly consider a boundary coupling that has a compact support on the spatial boundary coordinates. We show

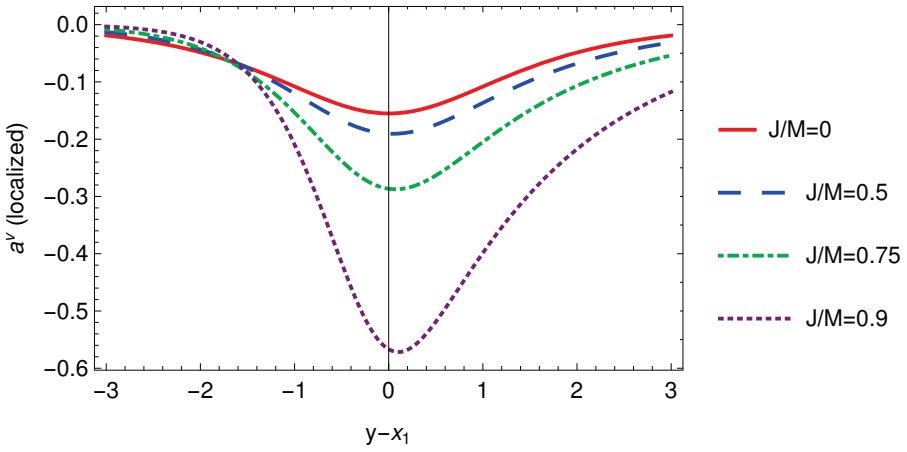

Figure 13: Opening of the wormhole when interaction is turned only along the x_1 direction. Temperature fixed $T = \frac{1}{2\pi}$. Set $g = 1$, $\Delta = 0.6$, $t_0 = 0$, and $t_f = 1$.

that this boundary profile of the coupling is reflected in the wormhole opening. There are many issues that remain to be explored in this fascinating subject:

- *Charge and extremality.* Given that our results show the rotation tends to make the wormhole larger, it is natural to ask what is the effect of charge in the size of the wormhole. A more detailed study either in the rotating or charged case would also be desirable.

- *Traversability in multi-boundary black holes.* In three dimensions multi-boundary black holes are constructed as an appropriate quotient of AdS. Their causal structure, entanglement entropy and complexity have been thoroughly studied [36–39]. It would be interesting to understand how traversability via a boundary deformation works in this scenario and to study its quantum teleportation interpretation.

- *Beyond the eikonal approximation.* Both [4] and [6] rely on the eikonal approximation [30, 31]. It would be interesting to investigate traversability by performing a scattering calculation that does not assume this approximation.

- *Testing reconstruction behind the horizon.* The traversable wormhole studied here implies a particular deformation of the boundary Hamiltonian. The effect of this deformation is to bring in causal contact the interior of the black hole and the boundary. Thus, standard reconstruction methods can now be used for operators that were in the black hole interior and this would allow to check the proposal of [40] for operators behind the horizon.

- *Higher dimensional wormholes.* Traversable wormholes obtained via double trace deformation have been studied so far only in $1+1$ and $2+1$ dimensions.

It would be nice to investigate what changes when we consider traversable wormholes in higher dimensions[7] in particular how the additional transverse directions can play a role from the boundary perspective as a quantum teleportation.

We hope to return to some of these issues in the future.

Acknowledgments

It is a pleasure to thank Jacques Distler and Don Marolf for enlightening conversations. E.C. and A.M. thank the ICTP-SAIFR for hospitality and the participants of the Latin American Workshop in Holography and Gravity (LAWGH) for stimulating discussions. This material is based upon work supported by the National Science Foundation under Grant Number PHY-1620610.

References

[1] N. Graham and K. D. Olum, *Achronal averaged null energy condition*, *Phys. Rev.* **D76** (2007) 064001 [0705.3193].

[2] W. R. Kelly and A. C. Wall, *Holographic proof of the averaged null energy condition*, *Phys. Rev.* **D90** (2014) 106003 [1408.3566].

[3] A. C. Wall, *Proving the Achronal Averaged Null Energy Condition from the Generalized Second Law*, *Phys. Rev.* **D81** (2010) 024038 [0910.5751].

[4] P. Gao, D. L. Jafferis and A. Wall, *Traversable Wormholes via a Double Trace Deformation*, *JHEP* **12** (2017) 151 [1608.05687].

[5] M. S. Morris, K. S. Thorne and U. Yurtsever, *Wormholes, Time Machines, and the Weak Energy Condition*, *Phys. Rev. Lett.* **61** (1988) 1446.

[6] J. Maldacena, D. Stanford and Z. Yang, *Diving into traversable wormholes*, *Fortsch. Phys.* **65** (2017) 1700034 [1704.05333].

[7] S. Sachdev and J. Ye, *Gapless spin fluid ground state in a random, quantum Heisenberg magnet*, *Phys. Rev. Lett.* **70** (1993) 3339 [cond-mat/9212030].

[8] A. Kitaev, *A simple model of quantum holography*, KITP strings seminar and Entanglement 2015 program, http://online.kitp.ucsb.edu/online/entangled15/.

[9] B. Czech, L. Lamprou and L. Susskind, *Entanglement Holonomies*, 1807.04276.

[10] J. De Boer, S. F. Lokhande, E. Verlinde, R. Van Breukelen and K. Papadodimas, *On the interior geometry of a typical black hole microstate*, 1804.10580.

[11] B. Yoshida and N. Y. Yao, *Disentangling Scrambling and Decoherence via Quantum Teleportation*, 1803.10772.

[7] See the recent paper [41]

[12] B. Yoshida and A. Kitaev, *Efficient decoding for the Hayden-Preskill protocol*, 1710.03363.

[13] A. Almheiri, A. Mousatov and M. Shyani, *Escaping the Interiors of Pure Boundary-State Black Holes*, 1803.04434.

[14] L. Susskind and Y. Zhao, *Teleportation Through the Wormhole*, 1707.04354.

[15] R. van Breukelen and K. Papadodimas, *Quantum teleportation through time-shifted AdS wormholes*, 1708.09370.

[16] D. Bak, C. Kim and S.-H. Yi, *Bulk View of Teleportation and Traversable Wormholes*, 1805.12349.

[17] M. Miyaji, *Time Evolution after Double Trace Deformation*, 1806.10807.

[18] M. Banados, M. Henneaux, C. Teitelboim and J. Zanelli, *Geometry of the (2+1) black hole*, *Phys. Rev.* **D48** (1993) 1506 [gr-qc/9302012].

[19] M. Banados, C. Teitelboim and J. Zanelli, *The Black hole in three-dimensional space-time*, *Phys. Rev. Lett.* **69** (1992) 1849 [hep-th/9204099].

[20] S. Hemming, E. Keski-Vakkuri and P. Kraus, *Strings in the extended BTZ space-time*, *JHEP* **10** (2002) 006 [hep-th/0208003].

[21] V. Balasubramanian and T. S. Levi, *Beyond the veil: Inner horizon instability and holography*, *Phys. Rev.* **D70** (2004) 106005 [hep-th/0405048].

[22] J. M. Maldacena, *Eternal black holes in anti-de Sitter*, *JHEP* **04** (2003) 021 [hep-th/0106112].

[23] C. Krishnan, *Tomograms of Spinning Black Holes*, *Phys. Rev.* **D80** (2009) 126014 [0911.0597].

[24] T. S. Levi and S. F. Ross, *Holography beyond the horizon and cosmic censorship*, *Phys. Rev.* **D68** (2003) 044005 [hep-th/0304150].

[25] I. Ichinose and Y. Satoh, *Entropies of scalar fields on three-dimensional black holes*, *Nucl. Phys.* **B447** (1995) 340 [hep-th/9412144].

[26] T. Azeyanagi, T. Nishioka and T. Takayanagi, *Near Extremal Black Hole Entropy as Entanglement Entropy via AdS(2)/CFT(1)*, *Phys. Rev.* **D77** (2008) 064005 [0710.2956].

[27] J. Maldacena, D. Stanford and Z. Yang, *Conformal symmetry and its breaking in two dimensional Nearly Anti-de-Sitter space*, *PTEP* **2016** (2016) 12C104 [1606.01857].

[28] S. H. Shenker and D. Stanford, *Black holes and the butterfly effect*, *JHEP* **03** (2014) 067 [1306.0622].

[29] S. H. Shenker and D. Stanford, *Stringy effects in scrambling*, *JHEP* **05** (2015) 132 [1412.6087].

[30] H. L. Verlinde and E. P. Verlinde, *Scattering at Planckian energies*, *Nucl. Phys.* **B371** (1992) 246 [hep-th/9110017].

[31] D. N. Kabat and M. Ortiz, *Eikonal quantum gravity and Planckian scattering*, *Nucl. Phys.* **B388** (1992) 570 [hep-th/9203082].

[32] T. Faulkner, R. G. Leigh, O. Parrikar and H. Wang, *Modular Hamiltonians for Deformed Half-Spaces and the Averaged Null Energy Condition*, *JHEP* **09** (2016) 038 [1605.08072].

[33] T. Andrade, S. Fischetti, D. Marolf, S. F. Ross and M. Rozali, *Entanglement and correlations near extremality: CFTs dual to Reissner-Nordström AdS_5*, *JHEP* **04** (2014) 023 [1312.2839].

[34] S. Leichenauer, *Disrupting Entanglement of Black Holes*, *Phys. Rev.* **D90** (2014) 046009 [1405.7365].

[35] Z. Fu, B. Grado-White and D. Marolf, *Toward self-supporting wormholes*, 1807.07917.

[36] S. Aminneborg, I. Bengtsson, D. Brill, S. Holst and P. Peldan, *Black holes and wormholes in (2+1)-dimensions*, *Class. Quant. Grav.* **15** (1998) 627 [gr-qc/9707036].

[37] V. Balasubramanian, P. Hayden, A. Maloney, D. Marolf and S. F. Ross, *Multiboundary Wormholes and Holographic Entanglement*, *Class. Quant. Grav.* **31** (2014) 185015 [1406.2663].

[38] V. Balasubramanian, J. R. Fliss, R. G. Leigh and O. Parrikar, *Multi-Boundary Entanglement in Chern-Simons Theory and Link Invariants*, *JHEP* **04** (2017) 061 [1611.05460].

[39] Z. Fu, A. Maloney, D. Marolf, H. Maxfield and Z. Wang, *Holographic complexity is nonlocal*, *JHEP* **02** (2018) 072 [1801.01137].

[40] A. Almheiri, T. Anous and A. Lewkowycz, *Inside out: meet the operators inside the horizon. On bulk reconstruction behind causal horizons*, *JHEP* **01** (2018) 028 [1707.06622].

[41] J. Maldacena, A. Milekhin and F. Popov, *Traversable wormholes in four dimensions*, 1807.04726.